The Spatial and Temporal Distribution of Organized Convective Structures over the Northeast and Their Ambient Conditions

KELLY A. LOMBARDO AND BRIAN A. COLLE

School of Marine and Atmospheric Sciences, Stony Brook University, Stony Brook, New York

(Manuscript received 15 April 2010, in final form 23 July 2010)

ABSTRACT

Organized convective structures over the northeastern United States were classified for two warm seasons (May–August) using 2-km composite radar [i.e., the National Operational Weather Radar (NOWrad)] data. Nine structures were identified: three types of cellular convection (clusters of cells, isolated cells, and broken lines), five types of linear convection (lines with no stratiform precipitation, lines with trailing stratiform precipitation, lines with parallel stratiform precipitation, lines with leading stratiform precipitation, and bow echoes), and one nonlinear system. The occurrence of all structures decreases from the western Appalachian slopes eastward to the Atlantic coast. Isolated cellular convection forms primarily during the morning to late afternoon (1200–2100 UTC) mainly over the high terrain. Clusters of cells form primarily over the Appalachians and the Atlantic coastal plain during the daytime (1200–0000 UTC). Linear convection is favored from midafternoon to early evening (1800–0000 UTC) over land areas. Nonlinear systems develop mainly from midafternoon to late evening (1800–0600 UTC) over the inland areas and over the coastal zone during the early morning (~1200 UTC).

Composites using the North American Regional Reanalysis (NARR) highlight the ambient conditions for three main convective structures: cellular, linear, and nonlinear. Cellular convection initiates with limited quasigeostrophic forcing and moderate instability [i.e., average most unstable CAPE (MUCAPE) ~973 J kg^{-1}]. A majority of cells develop in orographically favored upslope areas. Linear convection organizes along surface troughs, supported by 900-hPa frontogenesis and an average ambient MUCAPE of ~1011 J kg^{-1}. Nonlinear convection organizes along warm fronts associated with larger-scale baroclinic systems, and the MUCAPE is relatively small (~207 J kg^{-1}).

1. Introduction

Convective storms often organize and evolve into a variety of structures throughout their life cycle. Over the northeastern United States, convective storm evolution can be strongly modified by the Appalachians, land–water coastal boundaries, and various urban centers. The influence of these various surfaces across the northeastern United States on the initiation, evolution, and decay of convection makes forecasting warm season convection a challenge. Improved forecasts of these storms require a good understanding of the frequency of convective structures, their evolution spatially and temporally, as well as the environmental conditions that support such structures over this topographically complex region.

Much of our understanding of convective storm structures has focused on the central United States (Maddox 1981; Smull and Houze 1985; Wakimoto et al. 1998), given the high frequency and severity of convection in this region during the warm season. For example, several studies have classified mesoscale convective systems (MCSs) across the central United States according to structure using satellite or radar data and noted their frequency of occurrence (Bluestein and Jain 1985; Blanchard 1990; Parker and Johnson 2000; Jirak et al. 2003; Gallus et al. 2008). Bluestein and Jain (1985) examined linear convective structures in Oklahoma and identified four organizational modes: broken line, back building, broken areal, and embedded areal. Parker and Johnson (2000) classified linear systems over the central United States according to the location of stratiform precipitation (i.e., trailing stratiform, leading stratiform, and parallel stratiform). Gallus et al. (2008, hereafter GSJ08) divided warm season convection across the central United States into nine morphologies: isolated cells (IC), clusters of cells

Corresponding author address: Kelly Lombardo, School of Marine and Atmospheric Sciences, Stony Brook University, Stony Brook, NY 11794-5000.
E-mail: kellyann.lombardo@gmail.com

DOI: 10.1175/2010MWR3463.1

(CC), broken lines (BL), squall lines with no stratiform rain (NS), squall lines with trailing stratiform rain (TS), squall lines with parallel stratiform rain (PS), squall lines with leading stratiform rain (LS), bow echoes (BE), and nonlinear systems (NL). No formal studies have looked at the climatology of these convective structures over the northeastern United States.

There have been a growing number of climatological studies describing convective storm frequency across the eastern United States. Zajac and Rutledge (2001) showed that the diurnal cycle of lightning activity was more pronounced along the Atlantic coastal plain from Florida to the Delmarva than the Appalachian high terrain. Orville and Huffines (2001) highlighted the decrease of cloud-to-ground lightning frequency from Florida to the northeastern U.S. coast, with fewer flashes over the Appalachian high terrain compared to the Atlantic coastal plain. Parker and Ahijevych (2007) found that over the east-central United States, the probability of convection (>40 dBZ) occurring at a point is maximized on either side of the Appalachian terrain, with a relative minimum over the crest. Using both radar and lightning data over the northeastern United States, Murray and Colle (2011) illustrated preferred regions of convection (>45 dBZ) over the windward and lee sides of the Appalachians and some of the major river valleys. During the peak in diurnal heating, the frequency of >45 dBZ convection maximizes over the Northeast inland areas. This convective maximum shifts to the coast and offshore over the Atlantic coastal waters during the evening and overnight. Wasula et al. (2002) found that on days with severe weather over interior eastern New York, cloud-to-ground lightning frequency was maximized within the Mohawk and Hudson River valleys, with twice as much lightning than the surrounding terrain.

Previous studies highlighted the frequency and spatial distribution of convective storms over the eastern United States, but there is little knowledge of the spatial and temporal distribution of developing convective structures (e.g., isolated cells, cluster of cells, linear, etc.) across this region. This study is the first to perform a climatology of convective structures across the Northeast and the environments that support each structural type. The frequency of convective structures across the Northeast provides some information about the likelihood for the development of a particular type, while understanding the ambient conditions that favor the development of each convective structure will allow forecasters to better anticipate the type of organized convective structure on any particular day. Thus, this study will address the following motivational questions:

- What are the temporal and spatial distributions of the various convective structures over the Northeast during the warm season?
- How does the initiation of these structures vary with respect to the diurnal cycle, the underlying complex terrain, and coastal boundaries?
- What are the ambient conditions that support the development of these convective structures?
- How does the distribution of convective structures over the Northeast compare with the Midwest?

Section 2 describes the data and methods used in this study. The climatological results and the ambient conditions are presented in sections 3 and 4. Northeast and Midwest convective structures are compared in section 5. Conclusions and future work are highlighted in section 6.

2. Data and methods

Convective structures were identified and classified across the Northeast (see Fig. 1 for region) for two warm seasons: 1 May–31 August 2007 and a second warm season of days randomly selected during 1 May–31 August 2002–06. After completing the analysis for the 2007 season, it was determined that an aggregate season was needed, since there are relatively large (30%–40%) interannual variations in storm frequency across the Northeast (Murray and Colle 2011). For example, for the season using multiple years, the authors chose 1 May data randomly from the five 1 May times available from 2002 to 2006. Starting on 1 May, each convective event over the Northeast was tracked from initiation to decay. A subsequent day from a different year was not selected until all convection across the Northeast decayed (e.g., if convection is observed continuously from 1 May to 3 May 2002, a new year will be selected starting 4 May). The subsequent day was manually selected to be sure that there was no ongoing convection at 0000 UTC of the new day. This ensures that the initiation and decay times and locations were documented for all convective elements included in the dataset. The number of days selected from each warm season from 2002 to 2006 was comparable.

The Northeast was subdivided into four geographical domains (Fig. 1): upslope (UP), high terrain (HT), east slope/coastal plain (CP), and coastal ocean (CO) in order to relate each convective structure to changes in surface properties. The western boundary of the UP domain is the U.S.–Canadian border. The western boundary of the CO domain is the Atlantic coastline. The boundaries for the UP, HT, and CP subregions do not match the surface terrain exactly; rather, the geometry was simplified to more easily bin the convective structures manually into a particular domain. Since the four domains are

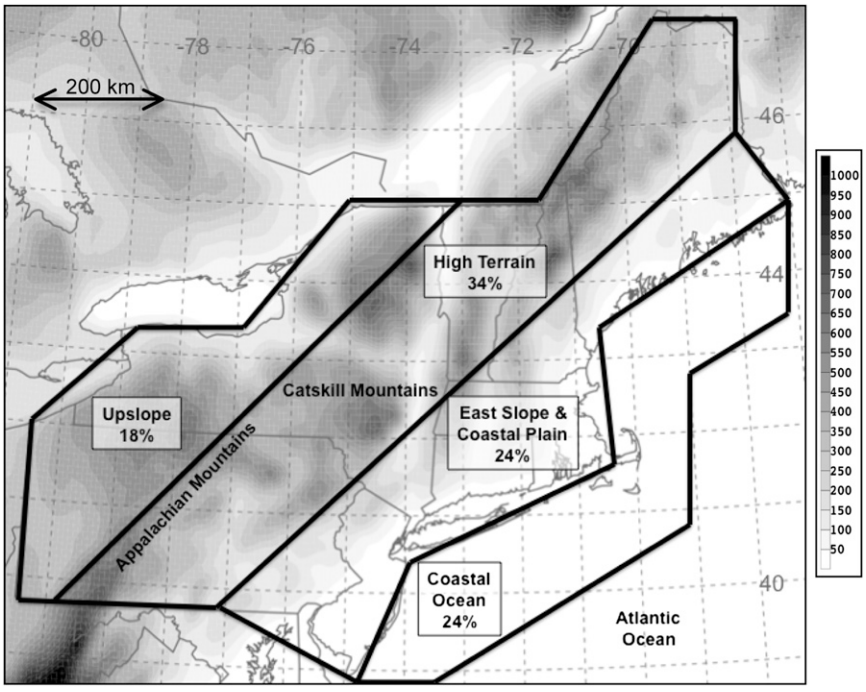

FIG. 1. The Northeast subdivided into four regions for the convective storm climatology. The fractional area of each subdomain with respect to the total Northeast area is indicated in percentage values. The terrain is shaded in meters.

not equivalent in size, the number of convective structures in each of the four regions was normalized by the fractional area that each domain covered relative to total of all four regions.

The convective structures were classified using the approach of GSJ08. All convective structures were identified manually using Weather Services International (WSI) National Operational Weather Radar (NOWrad) images available every 15 min at 2-km grid spacing. This manual approach has been applied to identify convective organizational structures in previous studies (Parker and Johnson 2000; Parker et al. 2001; Jirak et al. 2003; GSJ08). GSJ08 used a ≥30-dBZ threshold for central Plains convection, but this relatively low threshold included too many frontal stratiform events over the Northeast. For this study, each convective element must reach a radar reflectivity ≥35 dBZ to be included in the climatology. The first occurrence and the decay times were also documented. The first occurrence time includes initiation (a convective element first reaches 35 dBZ), when one convective type converts to another type (and ≥35 dBZ), or when a convective type moves into the Northeast domain (e.g., north, south, west, and east boundaries of Fig. 1). The decay time occurs when the convection is <35 dBZ.

Figure 2 illustrates examples of these structures, including (Fig. 2a) CC and a bow echo (BE), (Fig. 2b) a linear system with TS and IC, (Fig. 2c) a linear system with PS, (Fig. 2d) a linear system with LS, (Fig. 2e) a linear system with NS and a NL, and (Fig. 2f) a BL. Isolated cells have only one radar reflectivity maximum over a 20 km × 20 km area surrounded by clear air, while a cluster of cells contain at least two radar reflectivity maxima within a minimum of a 20 km × 20 km area, with weaker precipitation (<35 dBZ) connecting these more intense cores. Linear systems must be at least 50 km in length and exhibit a continuous line of ≥35-dBZ radar reflectivity with a length to width ratio of 5:1. Nonlinear systems have connected reflectivity maxima of ≥35 dBZ, with a length to width ratio of less than 5:1. For all convective organizational modes, each individual convective structure must be separated by 50 km from an adjacent convective structure by clear air (i.e., 0-dBZ radar reflectivity) and maintain its structure for a minimum of 30 min. As noted above, each time a convective group (i.e., clusters of cells) or element (i.e., linear system) organizes into a different structure, the formation of that new structure is catalogued as a new convective type with a new initiation location and time. For example, if clusters of cells initiate over the high terrain, move eastward and evolve into a linear system over the coastal plain, it is documented that a linear system developed over the coastal plain with the appropriate time.

To highlight the environments associated with the three main structural types (cellular, linear, and nonlinear),

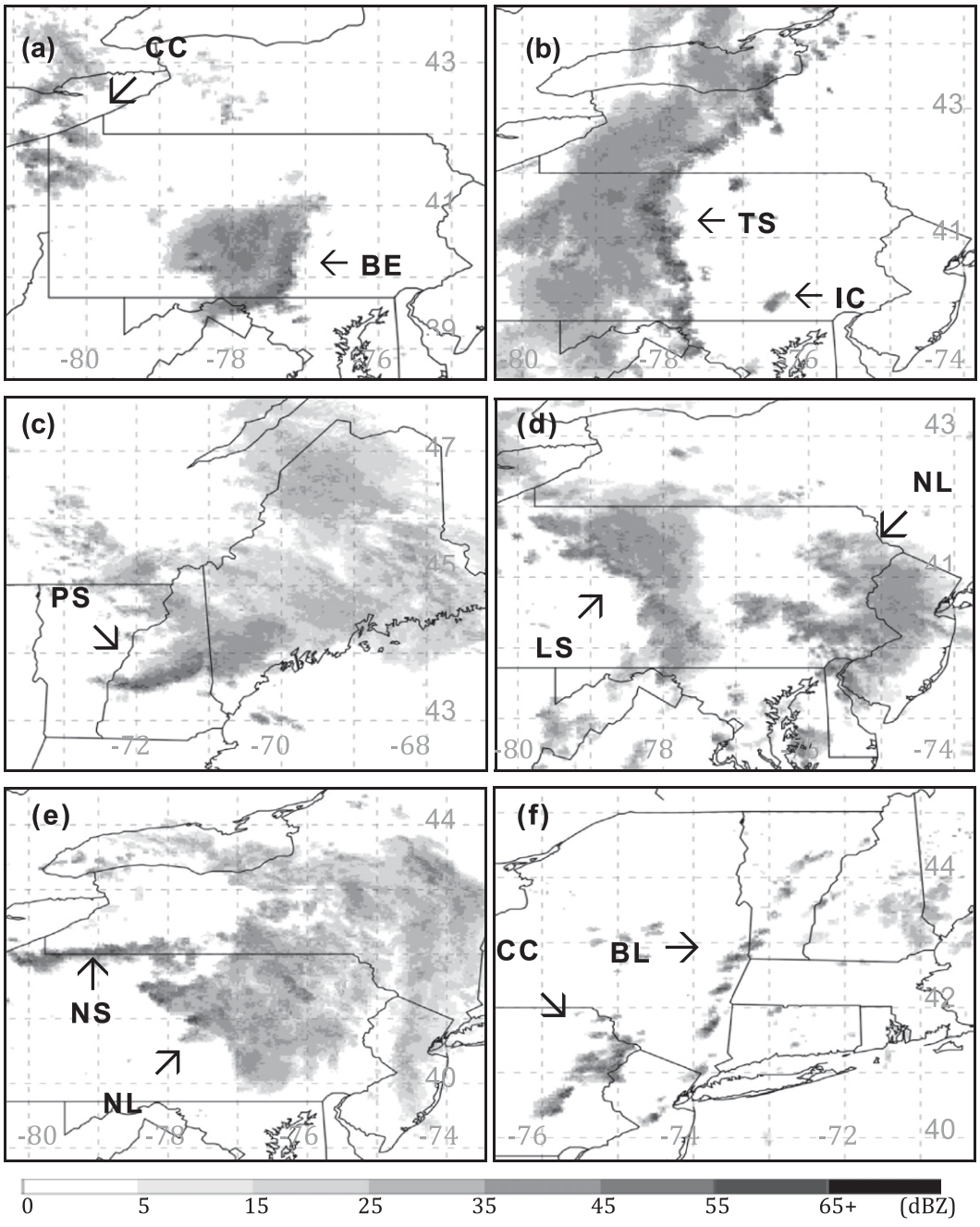

FIG. 2. NOWrad reflectivity (shaded every 5 dBZ) at 2-km grid spacing showing (a) clusters of cells (CC) and bow echo (BE) at 1545 UTC 9 Aug 2007, (b) linear system with trailing stratiform precipitation (TS) and isolated cells (IC) at 2345 UTC 8 Jun 2007, (c) linear system with parallel stratiform precipitation (PS) at 1815 UTC 9 Jul 2007, (d) linear system with leading stratiform precipitation (LS) and nonlinear system (NL) system at 1230 UTC 12 Jul 2004, (e) linear system with no stratiform precipitation (NS) and nonlinear system (NL) system at 0145 UTC 8 Aug 2007, and (f) broken line (BL) and clusters of cells (CC) at 1715 UTC 12 Jun 2007.

feature-based composites were constructed using the North American Regional Reanalysis (NARR) at 32-km grid spacing (Mesinger et al. 2006). The evolution of the most unstable CAPE (MUCAPE) and 1000-hPa equivalent potential temperature θ_e is presented to highlight the differing thermodynamic conditions among the three main structural types. For this study, the MUCAPE uses a parcel with the maximum θ_e in each 30-hPa

TABLE 1. List of dates used in the NARR composite for the cellular, linear, and nonlinear convective storm events. These include only those events with at least 90% of the convection over the Northeast exhibiting one particular organizational type (i.e., cellular, linear, or nonlinear).

Cellular events	Linear events	Nonlinear events
1500 UTC 21 May 2002	1800 UTC 12 May 2002	0900 UTC 14 Jun 2002
1800 UTC 27 May 2002	2100 UTC 31 May 2002	1200 UTC 9 May 2003
1500 UTC 9 Jun 2002	1800 UTC 12 Jun 2002	0600 UTC 24 May 2003
1800 UTC 25 Jun 2002	2100 UTC 21 Jun 2002	0600 UTC 26 May 2003
1800 UTC 2 Jul 2002	2100 UTC 27 Jun 2002	1200 UTC 11 Jun 2003
2100 UTC 3 Jul 2002	1800 UTC 23 Jul 2002	1800 UTC 20 Jun 2003
1500 UTC 18 Jul 2002	0600 UTC 28 Jul 2002	0600 UTC 3 Jul 2003
1800 UTC 31 Jul 2002	1800 UTC 2 Aug 2002	0000 UTC 11 Jul 2003
2100 UTC 1 Aug 2002	2100 UTC 21 Jul 2003	0000 UTC 16 Jul 2003
1800 UTC 3 Aug 2002	1800 UTC 16 Aug 2003	0300 UTC 29 Jul 2003
1800 UTC 13 Aug 2002	1800 UTC 26 Aug 2003	0600 UTC 1 Aug 2003
1800 UTC 17 Aug 2002	1500 UTC 14 May 2004	1200 UTC 28 May 2004
1500 UTC 18 Aug 2002	2100 UTC 18 May 2004	0900 UTC 5 Jun 2004
1800 UTC 9 Jun 2003	0300 UTC 23 May 2004	1800 UTC 13 Jun 2004
1800 UTC 27 Jun 2003	1500 UTC 24 May 2004	0900 UTC 22 Jun 2004
1800 UTC 29 Jun 2003	2100 UTC 9 Jun 2004	0900 UTC 12 Jul 2004
1800 UTC 8 Jul 2003	0900 UTC 14 Jul 2004	0900 UTC 26 Jul 2004
1500 UTC 25 Jul 2003	2100 UTC 29 Aug 2004	0000 UTC 15 Aug 2004
1500 UTC 12 Aug 2003	1500 UTC 5 Aug 2005	0900 UTC 8 Aug 2005
1500 UTC 13 Aug 2003	2100 UTC 30 May 2006	0900 UTC 16 Aug 2005
1800 UTC 11 May 2004	1800 UTC 2 Jul 2006	0600 UTC 18 Aug 2005
1800 UTC 17 May 2004	0000 UTC 11 Jul 2006	0000 UTC 20 Aug 2005
1800 UTC 30 Jun 2004	1800 UTC 28 Jul 2006	0600 UTC 28 Aug 2005
1500 UTC 1 Jul 2004	0600 UTC 30 Jul 2006	0000 UTC 5 May 2006
0000 UTC 18 Aug 2004	1800 UTC 3 Aug 2006	1500 UTC 6 May 2006
1500 UTC 18 Jul 2005	1500 UTC 10 May 2007	0900 UTC 21 May 2006
1800 UTC 4 Aug 2005	1500 UTC 16 May 2007	0600 UTC 4 Jul 2006
1500 UTC 10 Aug 2005	2100 UTC 8 Jun 2007	0600 UTC 12 Jul 2006
1500 UTC 11 Aug 2005	1800 UTC 13 Jun 2007	1500 UTC 22 Jul 2006
1500 UTC 22 Aug 2005	2100 UTC 19 Jun 2007	2100 UTC 14 Aug 2006
1500 UTC 3 Jul 2006	1500 UTC 27 Jun 2007	1800 UTC 19 Aug 2006
1500 UTC 26 Jul 2006	1800 UTC 28 Jun 2007	2100 UTC 1 May 2007
1500 UTC 31 Jul 2006	1500 UTC 5 Jul 2007	0600 UTC 15 May 2007
1500 UTC 1 Aug 2006	0900 UTC 9 Jul 2007	0900 UTC 6 Jun 2007
1800 UTC 23 May 2007	1500 UTC 11 Jul 2007	2100 UTC 30 Jun 2007
1800 UTC 24 May 2007	1800 UTC 15 Jul 2007	0900 UTC 4 Jul 2007
1500 UTC 25 May 2007	1800 UTC 27 Jul 2007	0600 UTC 18 Jul 2007
1800 UTC 10 Jun 2007	1500 UTC 9 Aug 2007	0900 UTC 19 Jul 2007
1800 UTC 17 Jun 2007		0600 UTC 23 Jul 2007
1800 UTC 25 Jun 2007		1500 UTC 7 Aug 2007
1500 UTC 26 Jun 2007		0600 UTC 13 Aug 2007
1500 UTC 10 Jul 2007		1200 UTC 19 Aug 2007
1500 UTC 16 Jul 2007		
1500 UTC 25 Jul 2007		
1800 UTC 28 Jul 2007		
1500 UTC 30 Jul 2007		
1800 UTC 8 Aug 2007		

layer from 0 to 180 hPa above the ground. Dynamical support for these structures is examined using 900-hPa Petterssen (1936) frontogenesis and 850-hPa temperature advection, as well as the evolving mid- and upper-level mass fields. Frontogenesis and temperature advection are examined at the levels at which the values are maximized.

The composite times include only those events during which at least 90% of the convection over the Northeast exhibits one particular organizational type (cellular, linear, or nonlinear). Composites included 47 cellular events, 38 linear events, and 42 nonlinear events during the 2007 and aggregate 2002–06 warm seasons (Table 1). Composites were centered on the location of the initiating

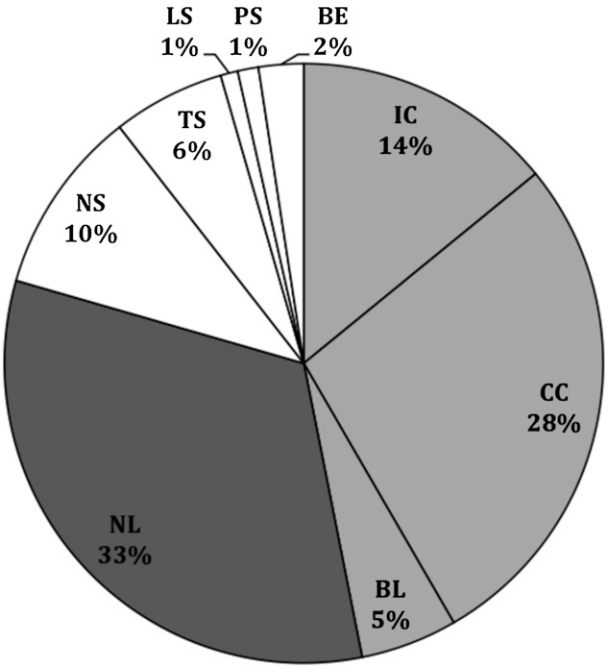

FIG. 3. The percentage distribution of the convective structures over the Northeast for the 2007 and aggregate 2002–06 warm seasons (May–August). Cellular, nonlinear, and linear events are light shaded, dark shaded, and not shaded, respectively.

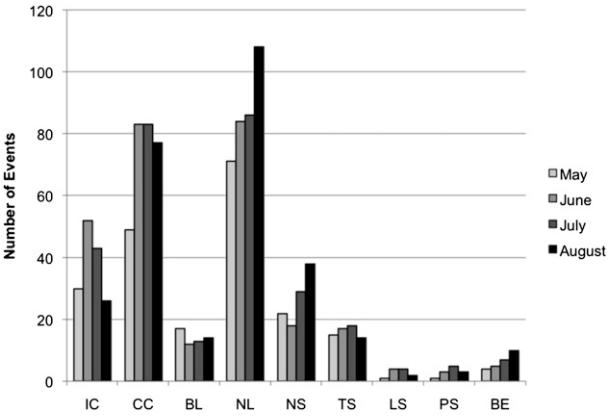

FIG. 4. Monthly occurrence of Northeast convective structures during the 2007 and aggregate 2002–06 warm seasons.

convection (feature based), which allowed for more robust synoptic and thermodynamic signals compared to geographically fixed composites. For linear and nonlinear convection, a point was selected ~0.75° (~85 km) ahead of the moving convection at the closest 3-h time prior to the most intense (in dBZ) convection. Choosing a point ahead of the moving convection limits convective contamination in the composites. Ongoing convection can alter the ambient environment immediately adjacent to the convection by 1) reducing the local CAPE, 2) decreasing the surface θ_e due to convective outflow, and 3) modifying the wind profile by local storm circulations. Cellular convection often does not move much horizontally, so choosing a point out ahead may not be representative of the conditions in which the cells are developing. Thus, for cellular events, the compositing point was the center of the initiating convection at the closest 3-h time prior to convective initiation. For all feature-based composite images, the center point of the feature-based composite is denoted as a star.

3. Distribution of convective structures and initiation

a. Warm season distribution

Figure 3 shows the percentage distribution of the nine convective structures across the northeastern United States for the 1071 convective elements included in this analysis. Of the three main organizational structures (i.e., cellular, linear, and nonlinear), cellular convection is the most common type, composing nearly half of all warm season convection. Within the cellular group, it is more common for cellular convection to organize into CC compared to IC. Supercells are categorized as ICs, suggesting that supercells are not common over the Northeast. NL systems make up one-third of all convective storms, while linear systems, the least common organizational type, develop only one-fifth of the time. Over the Northeast, half of the linear systems that develop have no associated stratiform precipitation, while about 30% are trailing stratiform systems.

The monthly distribution of each structure was also examined (Fig. 4). Both BL and IC develop more often during the early warm season months of May and June, respectively. The remaining organizational structures preferentially develop later in the warm season from mid- to late summer. Clusters of cells are equally as common from June through August. Nonlinear and two types of linear convection (NS and BE) develop more frequently during the late summer months, especially August. The remaining linear systems (TS, PS, and LS) do not show a preference for development during any part of the warm season, perhaps because of the more limited sample size.

b. Spatial variations and initiation

A Hovmöller plot shows the frequency of occurrence for isolated cells, cluster of cells, and linear and nonlinear types as a function of time of day across the four regions of the Northeast (Fig. 5). For the results presented herein, occurrence or development of a convective type is defined as the time it initiates, organizes into that type from a different convective structure, or

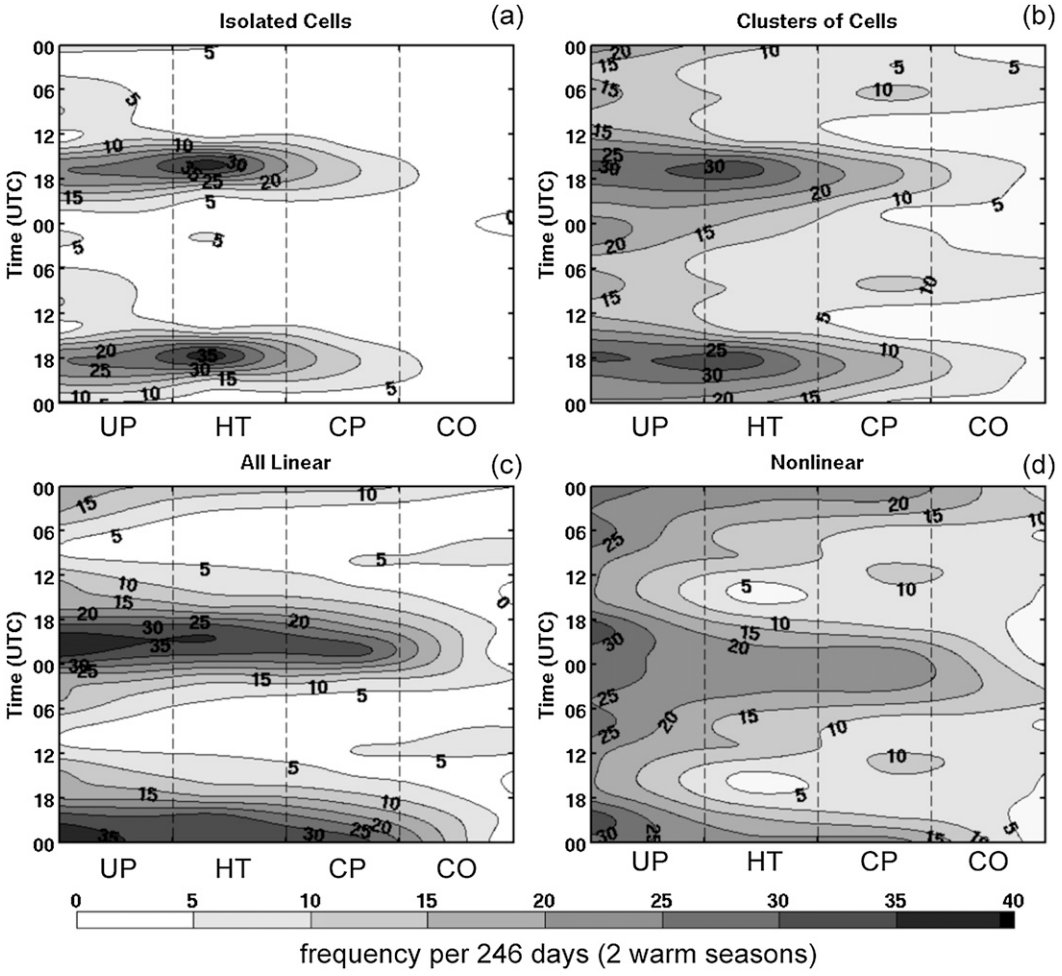

FIG. 5. Hovmöller plot of the number of initiation events over two warm seasons as a function of time of day (UTC) and region for (a) isolated cells, (b) clusters of cells, (c) all linear systems, and (d) nonlinear systems. Events are summed for both warm seasons (246 days) and normalized to account for variations in the region size.

enters into a region in Fig. 1 from outside the Northeast domain. All linear systems are grouped into one category (including BL) in order to increase sample size.

Two-thirds of all ICs occur from the morning into the late afternoon (1200–2100 UTC) over the land areas, with maximum development over the high terrain (Fig. 5a). The formation of CCs is maximized during approximately the same time frame (1200–0000 UTC) as ICs and occurs mainly over the upslope and high terrain regions (48% of all CC initiation; Fig. 5b). Unlike ICs, there is a small secondary maximum in CC development over the coastal plain in the early morning hours (0600–1200 UTC). Over the upslope and high terrain regions, the CCs may form during any time of the day, with their development decreasing from the high terrain region eastward to the coastal ocean.

Approximately two-thirds of all linear systems initiate between the late afternoon and early evening (1800–0000 UTC) over the land areas (Fig. 5c), about 6 h later than cellular development (IC and CC). There is almost no linear development during the early morning hours (0600–1200 UTC). Nonlinear systems primarily (61%) organize during the afternoon into the overnight hours (1800–0600 UTC) over all domains (Fig. 5d), which is ~3–6 h later than the linear systems. There is a secondary peak in nonlinear organization at 1200 UTC near the coastline. Similar to linear systems and cellular clusters, NL initiation is maximized over the Appalachian upslope and declines eastward toward the coastal ocean.

Figure 6 compares the number of developing convective structures within each of the four domains throughout the diurnal cycle. About 41% of all Northeast convective structures (596 of 1451 events) develop over the upslope domain (Fig. 6a). This percentage decreases over the high terrain (27%) and coastal plain (24%), decreasing dramatically over the coastal ocean

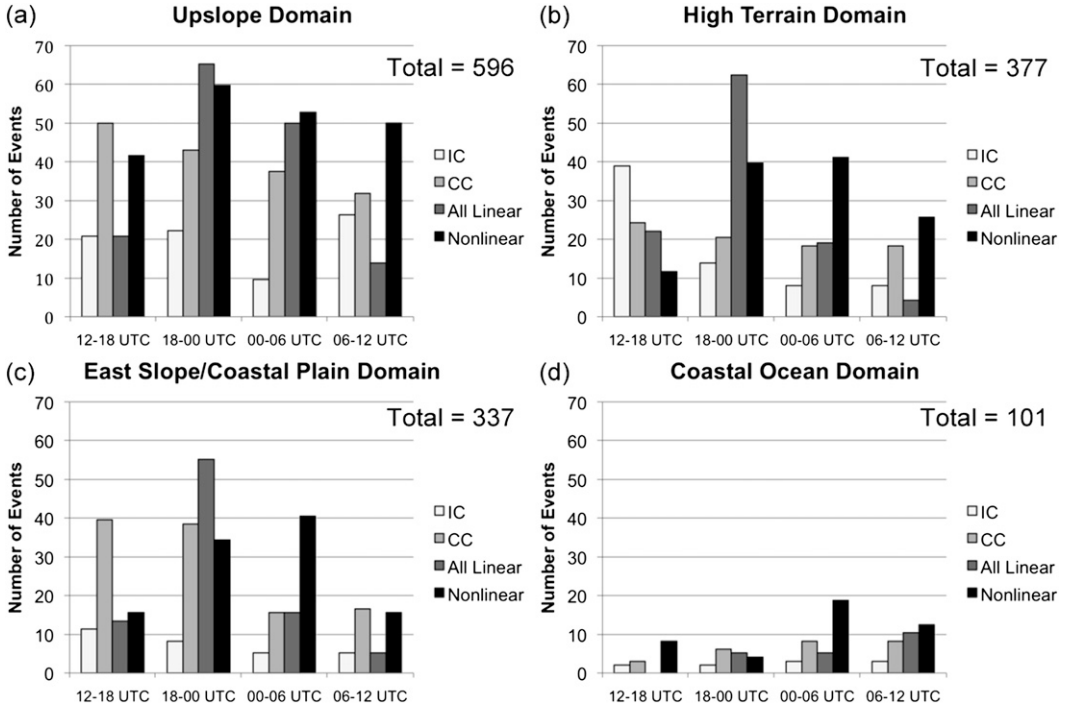

FIG. 6. Number of events initiated for the IC, CC, all linear, and NL structures summed for each 6-h period during the day (in UTC) for the (a) upslope, (b) high terrain, (c) east slope/coastal plain, and (d) coastal ocean regions in Fig. 1. The number of events is summed for both warm seasons and normalized to account for variations in region size.

(7%). The peak in the frequency of occurrence over the upslope region is partially a reflection of upstream convection moving into the domain from the west. Manual inspection of all convective events entering the boundaries of the four domains in June 2007 suggests that approximately the same number of convective systems move into the high terrain domain as the upslope domain. Thus, the upslope domain is the most active of the four domains for convection developing in situ.

Over the upslope region (Fig. 6a), during the morning and early afternoon hours (1200–1800 UTC), CCs and NL are the most common convective structures. By the late afternoon and early evening (1800–0000 UTC), linear and nonlinear systems develop most often. The frequency of initiation declines slightly into the early nighttime (0000–0600 UTC), with linear and nonlinear systems remaining the most common. The total storm initiation declines into the nighttime and early morning hours (0600–1200 UTC), and nonlinear convection becomes the dominant organizational structure (41% of the total structures). Throughout the day over this region, there is a progression of the dominant initiating type from cellular and nonlinear in the morning, to linear and nonlinear in the afternoon/evening, to primarily nonlinear during the nighttime. This evolution from cellular clusters to more linear and nonlinear systems is also apparent over the high terrain and coastal plain regions (Figs. 6b,c). However, in the morning, there is less developing nonlinear convection over these two regions, with ICs over the high terrain domain rather than CCs. The high terrain and coastal plain are also dominated by nonlinear systems in the evening (0000–0600 UTC).

The diurnal evolution of convection is much different over the coastal ocean. Nonlinear convection is the most common organizational structure during the day, with the exception of the late afternoon and early evening hours (1800–0000 UTC). During this time, all convective structures develop at approximately the same frequency.

4. Synoptic patterns and thermodynamic environments associated with convective structures

a. Cellular convective events

Figure 7 shows a series of spatial composites centered on the developing convection, illustrating the synoptic evolution for cellular (IC and CC) events, from 24 h before a cellular structure develops ($t - 24$ h) to the time of cell development ($t - 0$ h). At $t - 24$ h (Fig. 7a), a westward extension of the Bermuda anticyclone is located ~1200 km to the southwest of the cellular point,

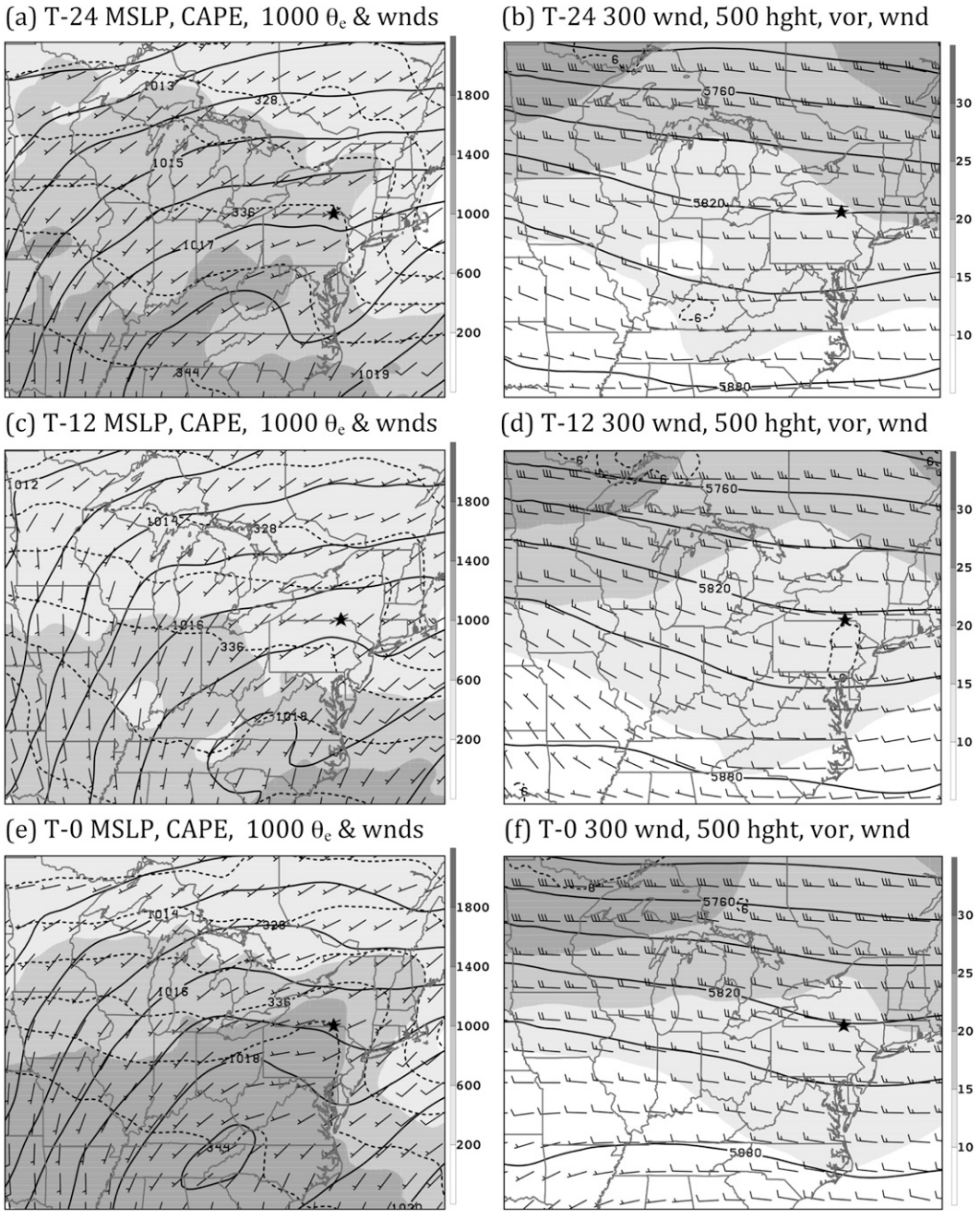

FIG. 7. Feature-based NARR composites for cellular convective events in Table 1 showing (a) MSLP (solid, every 1 hPa), 1000-hPa θ_e (dashed, every 4 K), MUCAPE (shaded, J kg^{-1}), and 1000-hPa wind (full barb = 5 m s^{-1}) at $t -$ 24 h and (b) 500-hPa heights (solid, every 30 dam), 500-hPa relative vorticity (dashed, every 6×10^{-5} s^{-1}), 300-hPa wind magnitude (shaded, m s^{-1}), and 500-hPa wind (full barb = 5 m s^{-1}) for $t - 24$ h. (c) As in (a), but for $t - 12$ h. (d) As in (b), but for $t - 12$ h. (e) As in (a), but for $t - 0$ h. (f) As in (b), but for $t - 0$ h. A star indicates the compositing point. Geography is included only for scale reference.

with a weak surface trough immediately east of this location. Southwesterly flow around the anticyclone advects warm and moist air ($\theta_e \sim 336$ K) air toward where the cell(s) first forms, with MUCAPE between 600 and 1000 J kg^{-1}. The core of the 20 m s^{-1} 300-hPa jet is ~1200 km poleward of the initiation point (Fig. 7b). A weak 500-hPa trough is located ~300 km to the west of the initiation point and the midlevel flow is nearly westerly. Inspection of many cases revealed that this nearly zonal flow in the composite is partially the result of the

cancellation of the exact position of the short-wave troughs, as well as the variety of flow regimes (northwesterly, southwesterly, and westerly) during these events. About 34% of cellular events develop in association with a midlevel short-wave trough.

By $t - 12$ h (Fig. 7c), there is little change in the surface pressure field (Fig. 7c), while MUCAPE decreases to <500 J kg^{-1} over the initiation point and the θ_e decreases to ~334 K. This composite time occurs during a diurnal minimum for many events, since 92% of cellular events develop between 1500 and 2100 UTC (Table 1). The 500-hPa trough is still ~300 km upstream of the initiation point, although it remains broad and weak (Fig. 7d).

At $t - 0$ h, the instability increases at the initiation point through daytime heating (MUCAPE $>$ 1000 J kg^{-1}), and the θ_e increases to 340 K (Fig. 7e). The precipitable water (32 mm) has increased little (~2 mm) over the previous 24 h (not shown). The surface trough to the east of the developing convection is more robust at this time (Fig. 7e). There is a weak 500-hPa trough axis centered where the cells first develop, so there is no vorticity advection, and the 300-hPa jet is displaced well to the north (Fig. 7f). As a result, there is little or no midlevel quasigeostrophic (**Q** vector) forcing (not shown). There is also little to no 850-hPa temperature advection where the cellular convection develops (Fig. 8a), and little frontogenetical forcing at 900 hPa (Fig. 8b).

Because there is limited synoptic forcing for ascent for these cellular events, it was hypothesized that upslope terrain forcing may provide a lifting mechanism. Figure 9 illustrates where the 47 cellular (IC and CC) convective events occurred over the Northeast with respect to four flow regimes at 900 hPa (045°–135°, 135°–225°, 225°–315°, and 315°–045°) obtained from the NARR dataset. From this analysis as well as the inspection of the individual events, ~60% of these cellular events develop along the terrain slopes in association with an upslope flow component. For example, westerly flow at 900 hPa (triangles) yields cellular initiation along western slopes and crest of the Pennsylvania Appalachians. Southerly flow (diamonds) favors cellular initiation on the southern and eastern slopes of the Catskill Mountains in south-central New York. Thus, orographic lift is an important lifting mechanism during a majority of the cellular events. The remainder of the cellular storms forms along or near a surface baroclinic zone (~25% of all cellular events, not shown), as well as along sea-breeze convergence zones over coastal New Jersey (~3 events).

b. Linear convective events

Figure 10 illustrates the composite synoptic evolution of all linear events from $t - 24$ h to the time of the most intense linear convection ($t - 0$ h) over the Northeast. At $t - 24$ h (Fig. 10a), a surface cyclone and trailing cold front is located ~1500 km to the northwest of where the linear system develops. There is enhanced MUCAPE (600–1000 J kg^{-1}) to the east of the surface front, which is associated with the northward advection of a surface θ_e ridge (~338 K) by southwesterly flow around an anticyclone off the southeastern U.S. coast (Fig. 10a). The 500-hPa flow over the linear convection point is west-northwesterly at 10 m s^{-1} as a result of a broad 500-hPa ridge ~600 km to the west (Fig. 10b). The 30 m s^{-1} 300-hPa jet core is centered ~1000 km poleward of the convection.

At $t - 12$ h (Fig. 10c), the surface cyclone and associated upper-level trough advance eastward to within ~1000 km of the linear convection point, while the 300-hPa jet gains a larger meridional flow component over the Great Lakes (Fig. 10d). Since 86% of the linear events included in the composites occur during the day (1500–0000 UTC; Table 1), the instability within the warm sector east of the surface front has decreased to ~600 J kg^{-1} (Fig. 10c) through nocturnal cooling. Warm advection shifts the θ_e gradient poleward of the linear convection point, while a surface trough begins to develop with a north–south-oriented axis over the convection location. This newly developing surface trough forms ~1000 km east of the surface cold front.

At $t - 0$ h (Fig. 10e), the trough to the east of the surface cold front has amplified (Fig. 10e), with linear convection organizing near the surface trough axis. It appears that linear events develop in association with a prefrontal surface trough ahead of a cold front. Examination of the individual events revealed that these prefrontal troughs are almost always located in the lee of the Appalachians. Manual inspection of these linear events suggests that the prefrontal troughs in the Appalachian lee develop from 1) adiabatic compressional (downslope) warming, 2) synoptic-scale ascent as the midlevel trough advances ahead of the surface cold front, or 3) a forward-tilting frontal structure, with the warmest mean tropospheric air and associated surface pressure trough located ahead of the surface front (Schultz and Steenburgh 1999; Schultz 2005).

Although linear systems can develop along prefrontal troughs, it is not as common as the composites might suggest, given the event averaging. During 40% of all linear events, there is a prefrontal/lee trough present, although the convection does not always organize within this trough. Manual inspection of the surface pressure maps revealed that ~22% of linear systems form within the axis of a prefrontal surface trough, while ~39% develop ahead of and within 300 km of a surface cold front, not within a surface trough. Furthermore, ~11% of

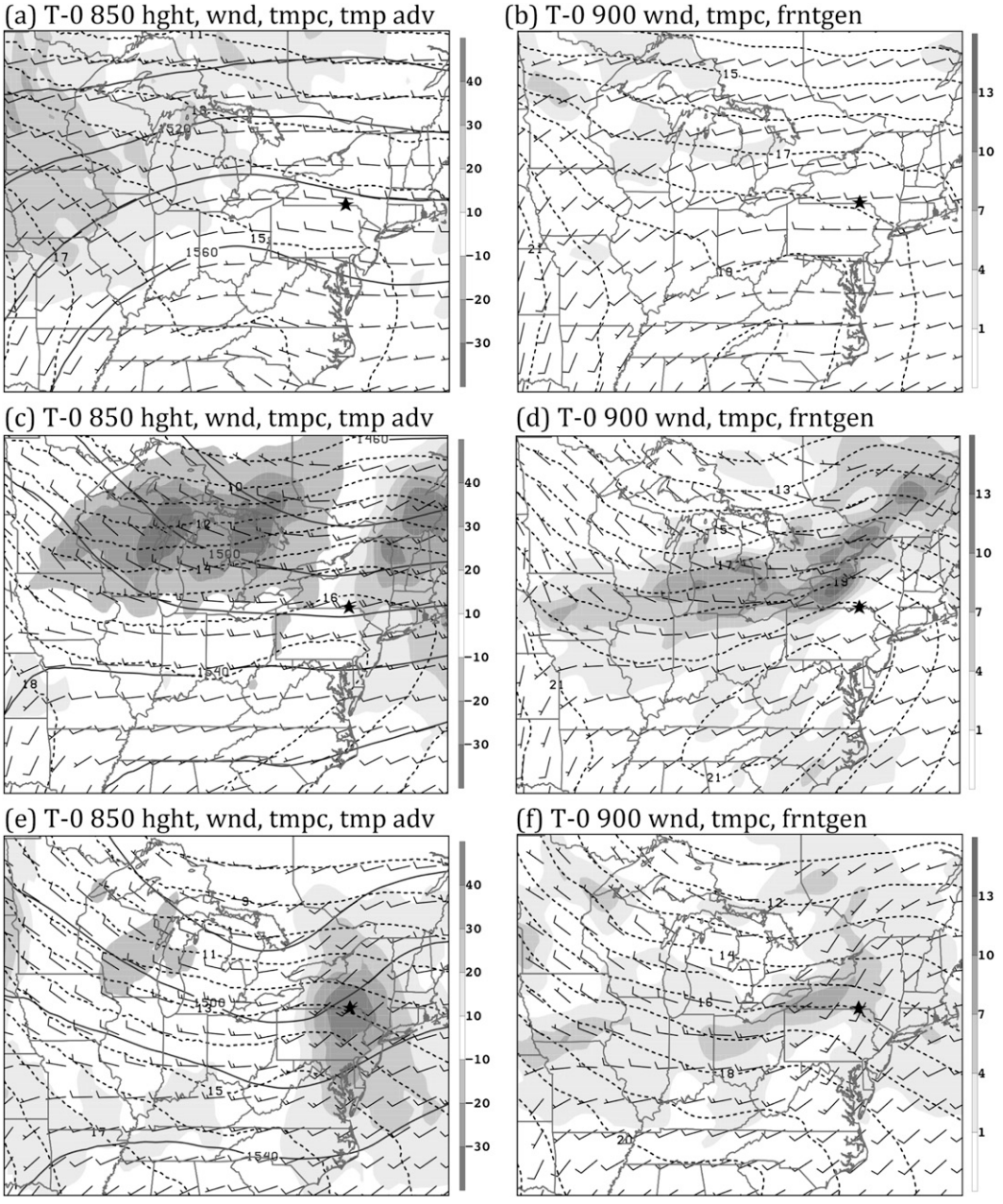

FIG. 8. Feature-based NARR composite for cellular convection at $t - 0$ h showing (a) 850-hPa heights (solid, every 20 dam), 850-hPa temperature (dashed, every 1°C), 850-hPa temperature advection (shaded, every 10×10^{-6} °C s^{-1}), and 850-hPa wind (full barb = 5 m s^{-1}) and (b) 900-hPa temperature (dashed, every 1°C), 900-hPa frontogenesis [shaded, every 3×10^{-2} K (100 km)$^{-1}$ (3 h)$^{-1}$], and 900-hPa wind (full barb = 5 m s^{-1}). (c) As in (a), but for linear events. (d) As in (b), but for linear events. (e) As in (a), but for nonlinear events. (f) As in (b), but for nonlinear events. A star indicates the compositing point. Geography is included only for scale reference.

the linear events form along a surface cold front within the associated surface trough, while ~17% form within the warm sector in the absence of any surface baroclinic zones in close proximity.

At $t - 0$ h (Fig. 10e), moist, unstable air advects to the northeast creating a wedge of relatively large MUCAPE (1000–1400 J kg^{-1}) and a θ_e ridge near the linear development. Meanwhile, the precipitable water values over the organizing convection have increased from 33 to 38 mm during the previous 24 h (not shown). A broad 500-hPa trough axis northwest of the convection trails the surface cyclone by ~600 km, while the amplifying

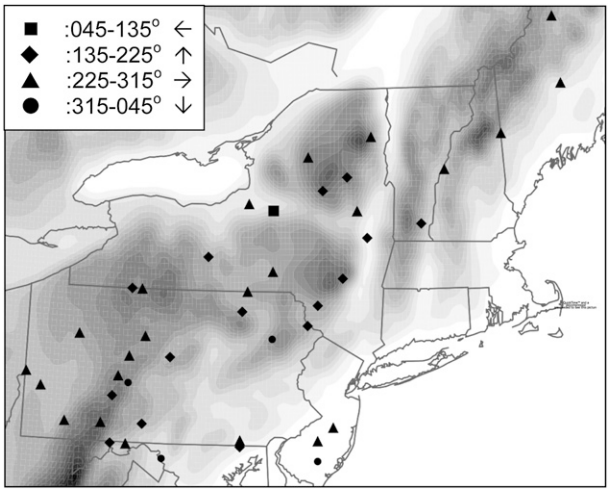

FIG. 9. The initiation locations for 47 cellular events (Table 1) with respect to Northeast topography (shaded, m). The initiation is subdivided by 900-hPa flow regime (a) 045°–135° wind direction = square, (b) 135°–225° = diamond, (c) 225°–315° = triangle, and (d) 315°–045° = circle.

300-hPa jet remains ~1000 km poleward of the linear convection (Fig. 10f). Given the locations of the 500-hPa trough and 300-hPa jet (Fig. 10f), there is weak **Q**-vector convergence (large-scale lift) from 700 to 500 hPa associated with the linear convection (not shown).

At 850 hPa for $t - 0$ h (Fig. 8c), the temperature advection is near zero over the developing convection, while there are relatively large warm and cold advections ($\pm 5.4 \times 10^{-1}$ °C h^{-1}) to the northeast and northwest of this point, respectively. Meanwhile, there is 900-hPa frontogenesis [$>10 \times 10^{-2}$ K (100 km)$^{-1}$ (3 h)$^{-1}$; Fig. 8d] located immediately northwest of the linear convection (Fig. 8d), suggesting that linear systems organize on the warm side of a 900-hPa frontogenesis maximum.

c. Nonlinear convective events

At $t - 24$ h prior to nonlinear convective events (Fig. 11a), a surface pressure ridge is located over the nonlinear convection development point, with a broad surface trough ~1500 km to the west. The lack of a well-defined surface trough is the product of compositing a variety of surface cyclone locations relative to the convection. The environment over the development location is weakly unstable (MUCAPE ~ 200 J kg^{-1}), with most of the instability >400 km equatorward. A meridionally orientated θ_e gradient extends from the Midwest to the East Coast. There is ~10 m s^{-1} of 500-hPa west-northwesterly flow and a 20 m s^{-1} 300-hPa jet over the nonlinear development location (Fig. 11b).

By $t - 12$ h, the broad surface trough advances eastward and is located over the Great Lakes, although there is little change in the ambient instability and thermal gradient as compared to 12 h earlier (Fig. 11c). The 500-hPa geopotential height field amplifies, as a mid-level trough deepens advancing toward the nonlinear composite point and the 25 m s^{-1} 300-hPa jet core broadens (Fig. 11d).

By $t - 0$ h, a more defined surface trough is located immediately west of the developing nonlinear convection, and the surface winds have veered to southerly ahead of this trough (Fig. 11e). Regardless, the instability remains equatorward, with MUCAPE of ~200 J kg^{-1} over the developing convection. The destabilizing of the atmosphere through diurnal heating is not required for nonlinear convection, since 57% of all nonlinear cases included in the composite develop between 0600 and 1200 UTC and the other 43% occur evenly between 1200 and 0600 UTC (Table 1). The precipitable water values have increased from 27 to 34 mm over the previous 12 h (not shown). The nonlinear system organizes along the surface baroclinic zone, with ~60% of the individual events included in this composite developing along a surface warm front (not shown). The 500-hPa trough continues to amplify as it approaches the developing convection (Fig. 11f). The 25 m s^{-1} 300-hPa jet shifts equatorward, placing the nonlinear convection in the right entrance region of the jet core, an area favorable for ascent and **Q**-vector forcing (not shown). Furthermore, 0–6-km shear over the developing NL convection has increased over the previous 12 h, with 1000-hPa winds rotating to from westerly to southerly as the surface trough encroaches on the developing convection in conjunction with a strengthening 500-hPa westerly flow (Figs. 11c–f).

At $t - 0$ h, 850-hPa temperature advection maximizes over the nonlinear convection, with values $>45 \times 10^{-6}$ °C s^{-1} (>1.6°C h^{-1}; Fig. 8e). Furthermore, the convection develops within a region of 900-hPa frontogenesis [6×10^{-2} K (100 km)$^{-1}$ (3 h)$^{-1}$] associated with a strengthening warm front to the east of the surface trough (Fig. 8f). Overall, nonlinear systems develop in association with strong forcing by an active baroclinic system and limited instability. The large areal coverage of nonlinear systems developing under strong dynamical forcing is consistent with Schumann and Roebber (2010). Examining the relationship between convective morphology and forcing by potential vorticity features on the dynamic tropopause, they found that the stronger the forcing, the more widespread the convection. Recall that the development of nonlinear systems is more evenly distributed over all four domains (UP, HT, CP, and CO) compared to the other organizational structures (cellular and linear; Fig. 5), indicating that these systems are the least influenced by the underlying topography.

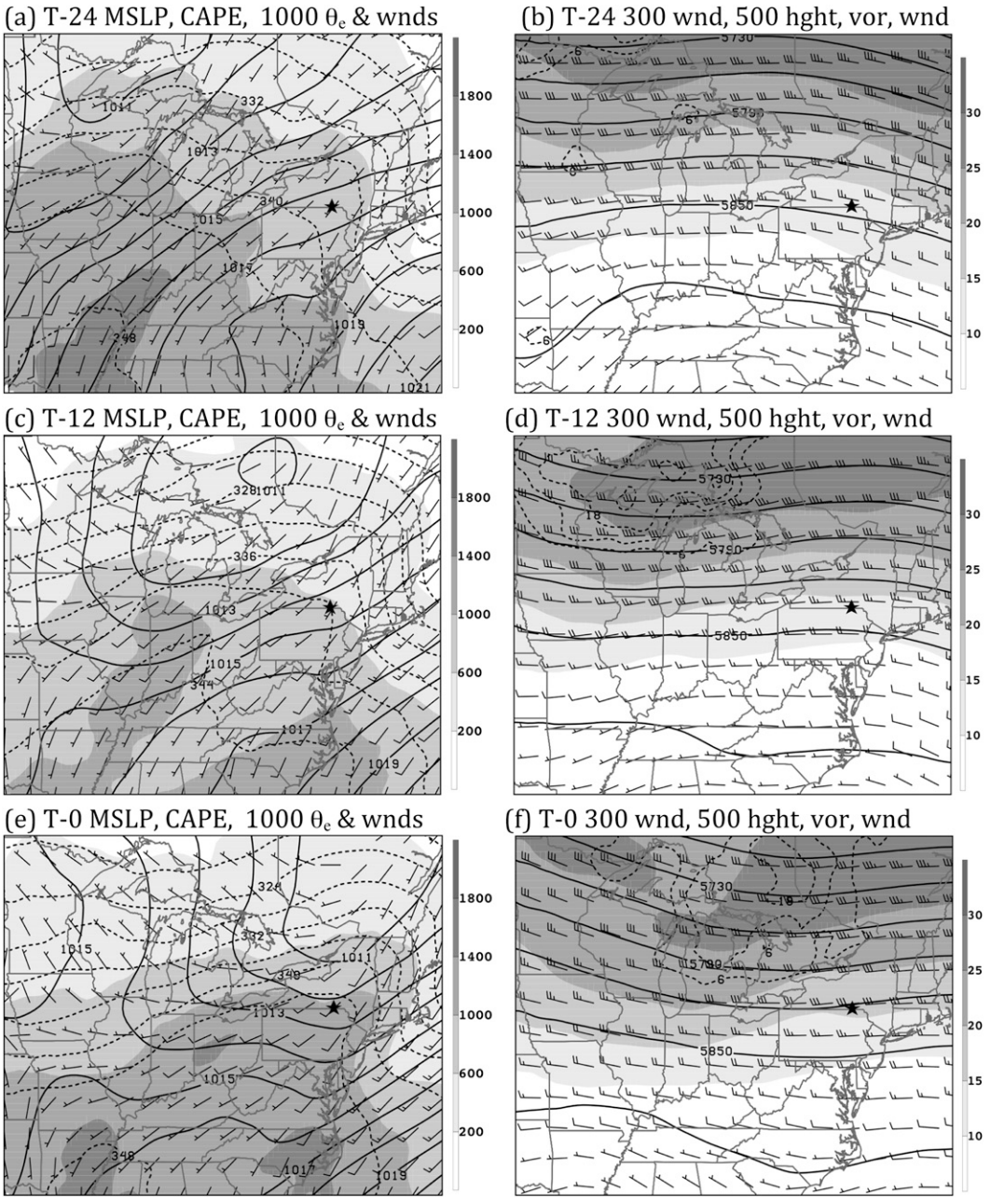

FIG. 10. Feature-based NARR composites for linear convective events in Table 1 showing (a) MSLP (solid, every 1 hPa), 1000-hPa θ_e (dashed, every 4 K), MUCAPE (shaded, J kg^{-1}), and 1000-hPa wind (full barb = 5 m s^{-1}) at $t -$ 24 h and (b) 500-hPa heights (solid, every 30 dam), 500-hPa relative vorticity (dashed, every 6×10^{-5} s^{-1}), 300-hPa wind magnitude (shaded, m s^{-1}), and 500-hPa wind (full barb = 5 m s^{-1}) for $t - 24$ h. (c) As in (a), but for $t - 12$ h. (d) As in (b), but for $t - 12$ h. (e) As in (a), but for $t - 0$ h. (f) As in (b), but for $t - 0$ h. A star indicates the compositing point. Geography is included only for scale reference.

5. Discussion

a. Comparison between organizational structures

To more quantitatively compare the physical processes among the convective structures (i.e., cellular, linear, and nonlinear), 1.5° latitude–longitude area-averaged values are calculated for a variety of variables centered on the compositing point, for each of the individual events included in the composites (Table 1). A bootstrap method (Zwiers 1990) was applied to the area-averaged variables to test for statistical significance between the three groups (i.e., cellular, linear, and nonlinear). For each variable,

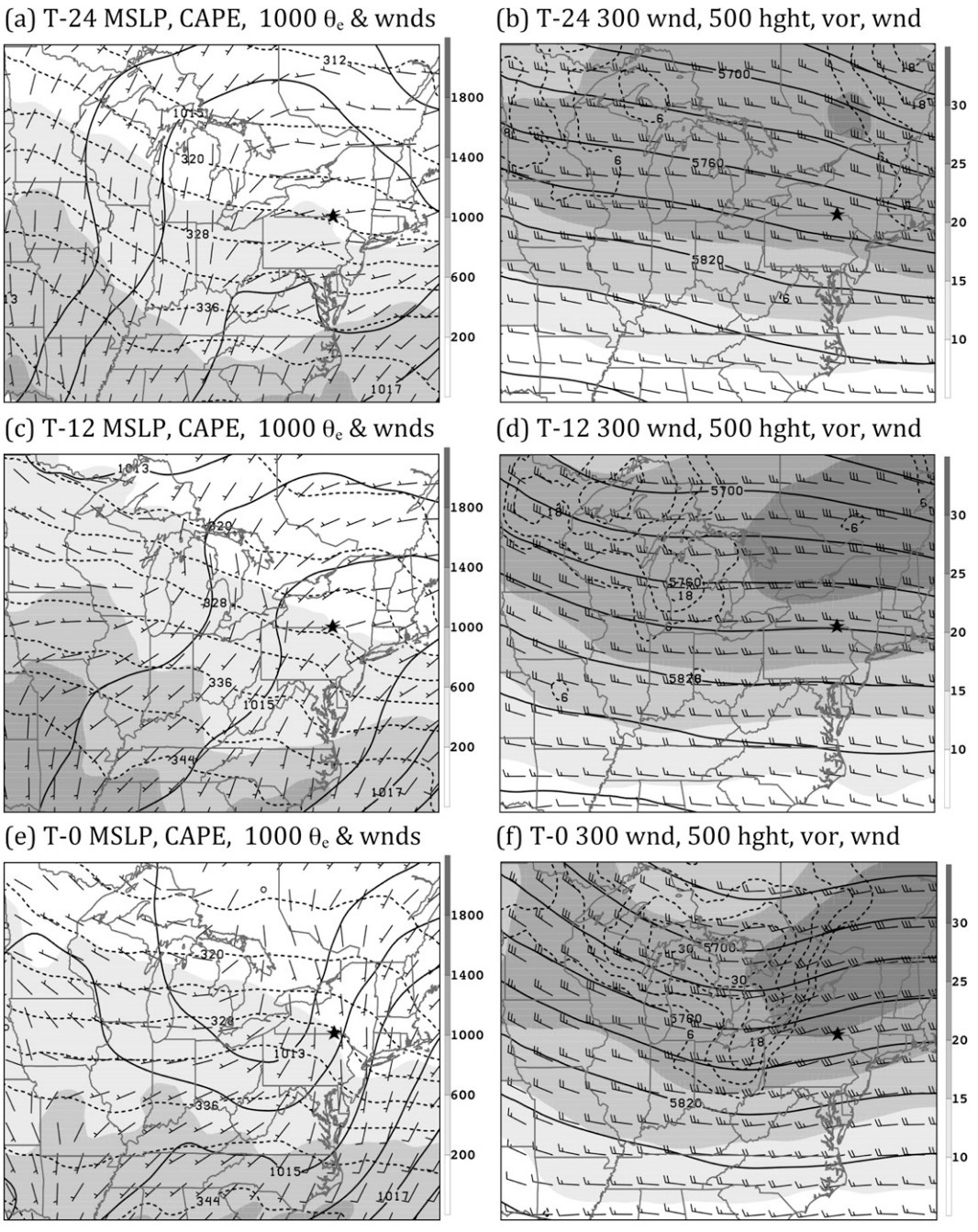

FIG. 11. As in Fig. 10, but for nonlinear events.

a new sample of the same size was generated 1000 times by randomly selecting from the original sample. The 95% confidence intervals around the mean were determined by finding the 2.5th and 97.5th percentile of the means of the 1000 resamples. The thermodynamic and dynamic quantities that support Northeast convective structures are also compared to Midwest and central Plains convective environments (Weisman and Klemp 1982; Parker and Johnson 2000; Coniglio et al. 2007).

Figure 12a illustrates the distribution of 900-hPa frontogenesis for the cellular, linear, and nonlinear events. The mean 900-hPa frontogenesis values for linear [11.6×10^{-2} K (100 km)$^{-1}$ (3 h)$^{-1}$] and nonlinear [13.1×10^{-2} K (100 km)$^{-1}$ (3 h)$^{-1}$] systems are significantly greater than cellular events [1.6×10^{-2} K (100 km)$^{-1}$ (3 h)$^{-1}$] at the

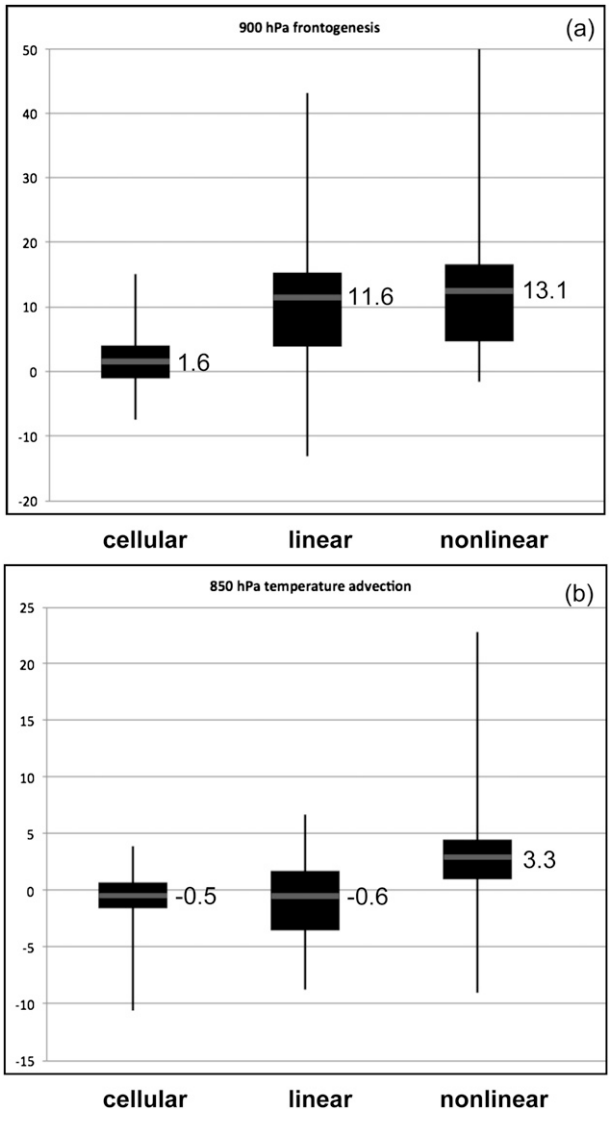

FIG. 12. Box-and-whisker plots showing (a) 900-hPa frontogenesis [10^{-2} K (100 km)$^{-1}$ (3 h)$^{-1}$] and (b) 850-hPa temperature advection (10^{-5} °C s^{-1}) for the 47 cellular events, 38 linear, and 42 nonlinear events in Table 1. The bottom and top of the solid black box are the 25th and 75th quartiles, respectively. The mean is denoted by a gray bar with its value also noted. The maximum and minimum outliers are denoted by the vertical solid lines.

95% level (not shown). A majority (~77%) of the cellular events that develop under frontolytical situations are forced by orographic lift over the Appalachian terrain, while the remaining events were supported by **Q**-vector forcing at midlevels (not shown). The tail in the distribution for nonlinear events is skewed toward stronger frontogenetical forcing, with values as high as 63.1×10^{-2} K (100 km)$^{-1}$ (3 h)$^{-1}$. Also, the mean 850-hPa warm air advection for nonlinear convective events (3.3×10^{-5} °C s^{-1} or 0.2°C h^{-1}) is significantly (95% level) larger than the near-neutral temperature advection during cellular (-0.5×10^{-5} °C s^{-1}) and linear (-0.6×10^{-5} °C s^{-1}) events (Fig. 12b).

The mean precipitable water value for linear convection (37.9 mm) is significantly greater than cellular (32.5 mm) and nonlinear (33.4 mm) convection at the 95% level (Fig. 13a). Furthermore, the spread of values is smaller for linear events, with values ranging from 27.4 to 48.7 mm, compared with cellular (9.3–45.7 mm) and nonlinear (14.19–46.43 mm) events. The middle 50% of precipitable water values (35.2–40.7 mm) for Northeast linear convection is greater than the average values for linear systems in the Great Plains (24.3–33.5 mm; Parker and Johnson 2000).

Both cellular and linear convection develop in moderate MUCAPE environments (Fig. 13b). The interquartile range for cellular convection is between 516–1124 J kg^{-1} and 754–1322 J kg^{-1} for linear convection (Fig. 13b). The MUCAPE values are similar to the central U.S. Plains during May, with mean values ranging from ~800 J kg^{-1} for the PS type to ~1600 J kg^{-1} for the TS system (Parker and Johnson 2000). However, there is a large spread in MUCAPE that support Northeast linear convection (196–2737 J kg^{-1}; Fig. 13b). In contrast, the interquartile CAPE range for nonlinear convection is 21–301 J kg^{-1}, while the mean (207 J kg^{-1}) is significantly (95% level) less than both cellular (973 J kg^{-1}) and linear (1112 J kg^{-1}) values. Furthermore, the maximum MUCAPE value associated with nonlinear events is only 1706 J kg^{-1}, which is substantially less that the maximum MUCAPE for linear (2737 J kg^{-1}) and cellular convection (3413 J kg^{-1}; Fig. 13b). Two events included in the nonlinear composites had an MUCAPE value of 0 J kg^{-1}, one of which was strongly and continuously forced by 850-hPa warm air advection and 900-hPa frontogenesis. This is consistent with the derecho work of Evans and Doswell (2001), who found that over the eastern two-thirds of the United States, strongly synoptically forced derechos associated with a deep midlevel trough and surface cold front can occur in environments with little to no CAPE. The other no MUCAPE event developed in association with relatively weak dynamical forcing (not shown), although there was potential instability present (1000–800 hPa).

It has been shown that the relationship between CAPE and shear is important for determining the structure of convection (Weisman and Klemp 1982, 1984; Rotunno et al. 1988; Weisman et al. 1988; Parker and Johnson 2000). Ambient shear over several depths was compared between the three convective types, with shear calculated as the magnitude of the vector difference over the layer. For 0–1-km shear, cellular convection forms in the smallest shear environments, with the middle 50% of

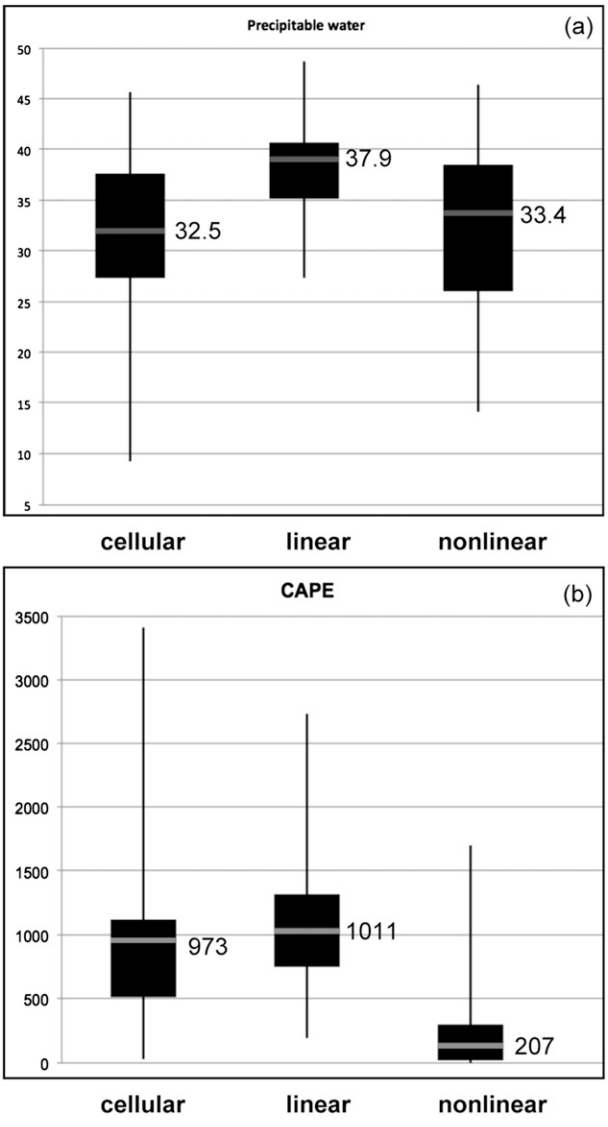

FIG. 13. As in Fig. 12, but for (a) precipitable water (mm) and (b) MUCAPE (J kg^{-1}).

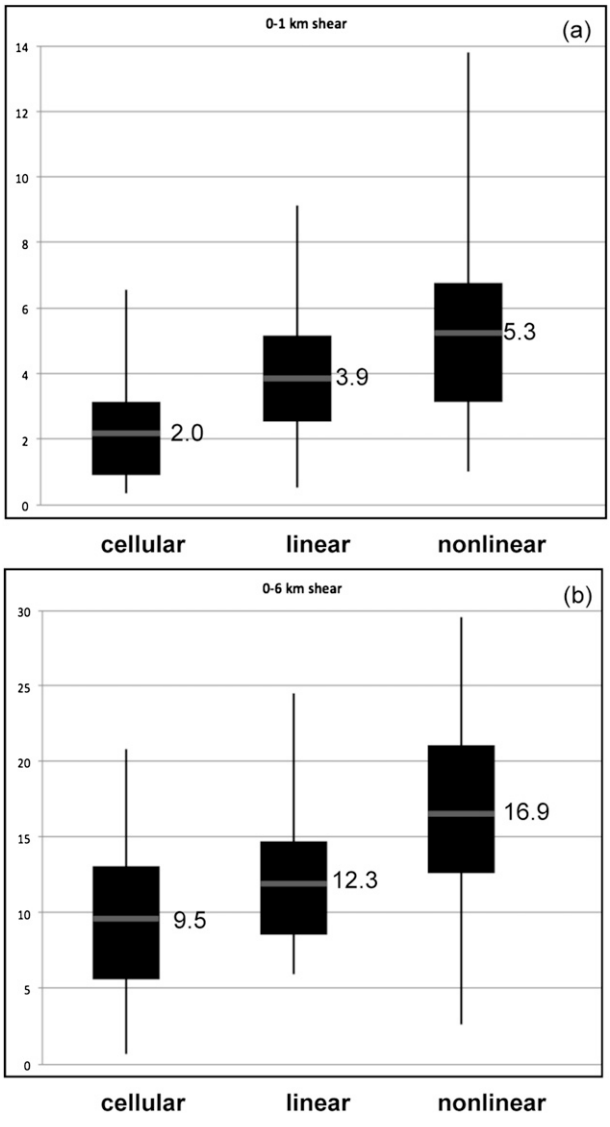

FIG. 14. As in Fig. 12, but for (a) 0–1-km shear (m s^{-1}) and (b) 0–6-km shear (m s^{-1}).

cellular events forming in 1–3 m s^{-1} of ambient shear (Fig. 14a). The interquartile range increases for linear convection (2.5–5.2 m s^{-1}) and more so for nonlinear convection (3.1–6.8 m s^{-1}). The mean values of 0–1-km shear for linear (3.9 m s^{-1}) and nonlinear systems (5.3 m s^{-1}) are significantly (95% level) greater than for the cellular convection (2.1 m s^{-1}). Furthermore, the mean 0–1-km shear for nonlinear systems is greater than for linear systems at the 90% significance level. The 0–3-km shear for linear and nonlinear convection is significantly (95% level) greater than cellular convection as well (not shown).

Mean values of 0–6-km shear for all three convective types are significantly different from each other at the 90% level, with a mean 0–6-km shear for cellular storms of 9.5 m s^{-1}, 12.3 m s^{-1} for linear systems, and 16.9 m s^{-1} for nonlinear events (Fig. 14b). The relatively weak deep layer shear during cellular events, with an interquartile range of 5.6–13.1 m s^{-1}, suggests that most northeastern U.S. cellular events are not supercellular (Fig. 14b). Through the use of proximity soundings, Thompson et al. (2003) found that the probability of supercells over the Midwest increases as the 0–6-km shear increases from 15 to 20 m s^{-1}. Though numerical simulations, Weisman and Klemp (1982) showed that for splitting cells to develop, the ambient 0–6-km shear must be a minimum of 20 m s^{-1}.

The middle 50% of linear events have 0–6-km shear values ranging from 8.6 to 14.8 m s^{-1}. There is little

difference between the 0–3- and 0–6-km shear values for linear systems (not shown), indicating that the greatest contribution to the ambient shear comes from winds below 3 km, consistent with Rotunno et al. (1988). About three-fourths of Northeast linear events included in this dataset have smaller 0–6-km shear values compared to all types of linear convective structures over the eastern half of the United States (Evans and Doswell 2001; Cohen et al. 2007; Coniglio et al. 2007), which ranged from 12 to 20 m s^{-1}.

In contrast, Northeast nonlinear systems have the greatest deep layer shear, with an interquartile range of 12.7–21.1 m s^{-1}, consistent with a well-defined baroclinic trough from the surface to midlevels (Figs. 11e,f). The 0–6-km shear vector during Northeast nonlinear events more closely resembles the shear values that support central U.S. quasi-linear systems (Evans and Doswell 2001; Cohen et al. 2007).

b. *Comparison between Northeast and Midwest convective types*

There are large differences in terrain between the Northeast and the central Plains, and the Atlantic coastal boundary adds another degree of complexity for the Northeast. These surface variations and associated ambient conditions (i.e., moisture, instability, and lift) will influence convective organizational structures over each region uniquely. To evaluate these differences, the structural distribution of convection over the Northeast (Fig. 3) is compared to the distribution over the Midwest highlighted by GSJ08.

Although the Northeast convective structures were classified according to the nine morphologies of GSJ08, the results cannot be compared directly since the analysis was completed manually by two separate research groups. Therefore, to compare our Northeast results with the GSJ08 analysis, we first classified the convective structures over the GSJ08 region of interest (i.e., Midwest) from 1 to 30 June 2002 using the same reflectivity data and approach described in section 2. We identified nearly twice as many convective structures across the Midwest compared to the GSJ08 analysis for that month. There are two reasons for this discrepancy (W. Gallus 2010, personal communication): 1) we classified all convective elements across the domain, while GSJ08 identified the dominant morphology over the Midwest during a particular time; and 2) we identified convective structures every 15-min, while GSJ08 identified them every hour. Since a goal is to obtain a qualitative comparison of the different structures between the Midwest and Northeast, the GSJ08 percentages of the various convective types were adjusted to account for these differences in classification. Two convective distributions for June 2002 were calculated, one using the classification of GSJ08 and the other using our approach. The percentage difference between these two June 2002 distributions was calculated (adjustment factor) and added to the total warm season structural distribution of GSJ08. This approach only provides a rough adjustment, so any differences noted between the two regions must be relatively large to be discussed.

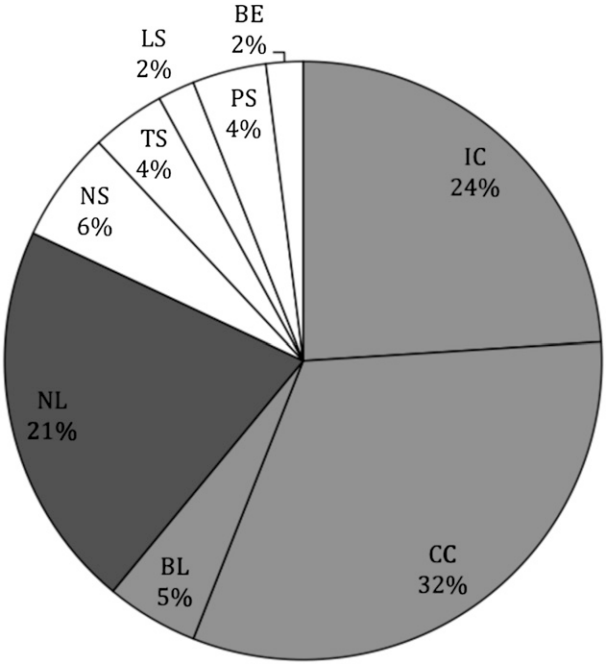

FIG. 15. Structural distribution of Midwest convective cases examined by Gallus et al. (2008) modified to account for the classification differences between this Northeast study and GSJ08. See text for details.

Figure 15 illustrates the full warm season (April–August 2002) GSJ08 distribution modified by the adjustment factor noted above. The greatest variations between the original GSJ08 distribution (GSJ08, their Fig. 6) and Fig. 15 are that the adjusted distribution has 8% fewer NLs and 12% more CCs. Thus, the difference between the original GSJ08 distribution and the adjusted GSJ08 distribution are relatively small, giving us additional confidence in comparing the adjusted GSJ08 distribution with our Northeast results.

The main structural differences between Northeast (Fig. 3) and Midwest (Fig. 15) convection exist in the percentage of NL and IC convection. During the warm season, there is a greater percentage of NL systems over the Northeast (33%) than the Midwest (20%). There is likely a larger number of baroclinic systems over the Northeast during the warm season compared to the central Plains. A smaller percentage of convection organizes into ICs over the Northeast (14%) compared to the Midwest (24%). This difference may reflect the more

frequent supercell development over the Midwest compared to the Northeast.

6. Summary

Using 2-km NOWrad reflectivity for two warm seasons (May–August), nine convective organizational structures were identified over the Northeast, including three types of cellular convection (isolated cells, cluster of cells, and broken lines), five types of linear convection (no stratiform, trailing stratiform, parallel stratiform, leading stratiform, and bow echoes), and one nonlinear system. Cellular events compose ~47% of all convective structures, nonlinear ~33%, and linear ~20%. Comparing the structural distribution of convection over the Northeast to the Midwest (GSJ08), fewer isolated cells develop over the Northeast (14%) compared to the Midwest (24%). Conversely, more nonlinear systems develop over the Northeast (33%) than the Midwest (21%).

Development of the various convective structures is dependent on the underlying terrain as well as the diurnal cycle. Two-thirds of all isolated cells form from the morning into the late afternoon (1200–2100 UTC) over the land areas, with a peak in convective initiation over the high terrain. Half of all cellular clusters develop from morning into the early evening (1200–0000 UTC) over the western Appalachian upslope, eastern Appalachian slopes, and Atlantic coastal plain, with a secondary maximum in development near the Atlantic coastline between 0600 and 1200 UTC. Two-thirds of all linear convection organizes from the midafternoon into the early evening (1800–0000 UTC) over the Northeast land areas. Approximately 60% of nonlinear systems organize across the entire domain during the midafternoon into the first half of the night (1800–0600 UTC), with a secondary peak in development near the Atlantic coastline around 1200 UTC.

Over the Northeast land areas, the dominant developing convective structure varies throughout the day, especially over the high terrain and coastal plain areas. In the morning and early afternoon hours (1200–1800 UTC), cellular convection is the most common developing organizational mode. The favored convective type transitions to linear systems during the late afternoon into the early evening (1800–0000 UTC). By the early evening into the overnight (0000–0600 UTC), nonlinear convection is the most common developing structure. The organization of convective structures is a minimum during the overnight into the morning hours (0600–1200 UTC).

Over the coastal ocean, the evolution of the developing convection is very different from the Northeast land areas. Only 7% of all convection structures organize over the coastal waters as opposed to the three inland domains, with a majority (40%) of the developing convection organizing into nonlinear structures. Though there is a minimum in convective initiation over the coastal ocean, the development of convection increases moving westward, with peak development occurring over the upslope domain.

Feature-based composites were used to diagnose the synoptic patterns and thermodynamic environments during warm season convective days when there is a dominant (>90%) convective mode (i.e., cellular, linear, and nonlinear) over the Northeast. Cellular convection develops within moderately unstable air (MUCAPE ~ 1000 J kg^{-1}), though the large-scale forcing for ascent during these events is weak at all levels. For cellular events, the primary lifting mechanism for ascent is orographic lift, caused by low-level upslope flow over the Appalachian terrain. Cells can also develop along seabreeze convergence zones in the Atlantic coastal plain.

Linear convection organizes on the warm side of a low-level frontogenesis maximum, within the axis of a surface trough. Near the developing linear convection, instability is modest with MUCAPE values ~1000 J kg^{-1} and θ_e values are high (~344 K). The deep layer (0–6 km) shear during these events is ~12.3 m s^{-1}, with most of the shear located in the lowest few kilometers.

Nonlinear convection is forced by relatively deep baroclinic systems, with the convection organizing along a strengthening baroclinic zone east of a surface trough. These systems are collocated with a maximum in low-level warm advection and the ascent region of the upper-level jet circulations. Supported by strong dynamical forcing, nonlinear systems form in environments with low MUCAPE (~200 J kg^{-1}).

The goal of this research is to better understand the evolution of Northeast convection in order to help increase the predictive skill for these systems. More detailed analysis is needed concerning the development and evolution of convection near terrain and the coastal plain in this region, such as the relative role of terrain in modifying baroclinic zones and low-level pressure patterns leading to environments conducive to convection. Even less is known about the interaction between convection and coastal boundaries of the East Coast, indicating that more work is required to understand the processes that control the evolution of convection over a marine environment.

Acknowledgments. This study was supported by the National Science Foundation under Grant ATM-0705036. We thank the three anonymous reviewers and Dr. David Schultz for their constructive comments that helped improve the manuscript.

REFERENCES

Blanchard, D. O., 1990: Mesoscale convective patterns of the southern High Plains. *Bull. Amer. Meteor. Soc.,* **71,** 994–1005.

Bluestein, H. B., and M. H. Jain, 1985: Formation of mesoscale lines of precipitation: Severe squall lines in Oklahoma during the spring. *J. Atmos. Sci.,* **42,** 1711–1732.

Cohen, A. E., M. C. Coniglio, S. F. Corfidi, and S. J. Corfidi, 2007: Discrimination of mesoscale convective system environments using sounding observations. *Wea. Forecasting,* **22,** 1045–1062.

Coniglio, M. C., H. E. Brooks, S. J. Weiss, and S. F. Corfidi, 2007: Forecasting the maintenance of quasi-linear mesoscale convective systems. *Wea. Forecasting,* **22,** 556–570.

Evans, J. S., and C. A. Doswell III, 2001: Examination of derecho environments using proximity sounding. *Wea. Forecasting,* **16,** 329–342.

Gallus, W. A., N. A. Snook, and E. V. Johnson, 2008: Spring and summer severe weather reports over the Midwest as a function of convective mode: A preliminary study. *Wea. Forecasting,* **23,** 101–113.

Jirak, I. L., W. R. Cotton, and R. L. McAnelly, 2003: Satellite and radar survey of mesoscale convective system development. *Mon. Wea. Rev.,* **131,** 2428–2449.

Maddox, R. A., 1981: Satellite depiction of the life cycle of a mesoscale convective complex. *Mon. Wea. Rev.,* **109,** 1583–1586.

Mesinger, F., and Coauthors, 2006: North American Regional Reanalysis. *Bull. Amer. Meteor. Soc.,* **87,** 343–360.

Murray, J., and B. A. Colle, 2011: The spatial and temporal variability of convective storms over the Northeast United States during the warm season. *Mon. Wea. Rev.,* in press.

Orville, R. E., and G. R. Huffines, 2001: Cloud-to-ground lightning in the United States: NLDN results in the first decade, 1989–98. *Mon. Wea. Rev.,* **129,** 1179–1193.

Parker, M. D., and R. H. Johnson, 2000: Organizational modes of midlatitude mesoscale convective systems. *Mon. Wea. Rev.,* **128,** 3413–3436.

——, and D. A. Ahijevych, 2007: Convective episodes in the east-central United States. *Mon. Wea. Rev.,* **135,** 3707–3727.

——, S. A. Rutledge, and R. H. Johnson, 2001: Cloud-to-ground lightning in linear mesoscale convective systems. *Mon. Wea. Rev.,* **129,** 1232–1242.

Petterssen, S., 1936: A contribution to the theory of frontogenesis. *Geofys. Publ.,* **11,** 1–27.

Rotunno, R., J. B. Klemp, and M. L. Weisman, 1988: A theory for strong, long-lived squall lines. *J. Atmos. Sci.,* **45,** 463–485.

Schultz, D. M., 2005: A review of cold fronts with prefrontal troughs and wind shifts. *Mon. Wea. Rev.,* **133,** 2449–2472.

——, and W. J. Steenburgh, 1999: The formation of a forward-tilting cold front with multiple cloud bands during Superstorm 1993. *Mon. Wea. Rev.,* **127,** 1108–1124.

Schumann, M. R., and P. J. Roebber, 2010: The influence of upper-tropospheric potential vorticity on convective morphology. *Mon. Wea. Rev.,* **138,** 463–474.

Smull, B. F., and R. A. Houze, 1985: A midlatitude squall line with a trailing region of stratiform rain: Radar and satellite observations. *Mon. Wea. Rev.,* **113,** 117–133.

Thompson, R. L., R. Edwards, J. A. Hart, K. L. Elmore, and P. Markowski, 2003: Close proximity soundings within supercell environments obtained from the Rapid Update Cycle. *Wea. Forecasting,* **18,** 1243–1261.

Wakimoto, R. M., C. Liu, and H. Cai, 1998: The Garden City, Kansas, storm during VORTEX 95. Part I: Overview of the storm's life cycle and mesocyclogenesis. *Mon. Wea. Rev.,* **126,** 372–392.

Wasula, A. C., L. F. Bosart, and K. D. LaPenta, 2002: The influence of terrain on the severe weather distribution across interior eastern New York and western New England. *Wea. Forecasting,* **17,** 1277–1289.

Weisman, M., and J. Klemp, 1982: The dependence of numerically simulated convective storms on vertical wind shear and buoyancy. *Mon. Wea. Rev.,* **110,** 504–520.

——, and ——, 1984: The structure and classification of numerically simulated convective storms in directionally varying wind shears. *Mon. Wea. Rev.,* **112,** 2479–2498.

——, ——, and R. Rotunno, 1988: Structure and evolution of numerically simulated squall lines. *J. Atmos. Sci.,* **45,** 1990–2013.

Zajac, B. A., and S. A. Rutledge, 2001: Cloud-to-ground lightning activity in the contiguous United States from 1995 to 1999. *Mon. Wea. Rev.,* **129,** 999–1019.

Zwiers, F. W., 1990: The effect of serial correlation on statistical inferences made with resampling procedures. *J. Climate,* **3,** 1452–1461.